# Amorphous NiCu Thin Films Sputtered on TiO$_2$ Nanotube Arrays: A Noble-Metal Free Photocatalyst for Hydrogen Evolution

Marco Pinna$^+$,[a, f] Angeline Wo Weng Wei$^+$,[b] Davide Spanu,[a] Johannes Will,[c] Tadahiro Yokosawa,[c] Erdmann Spiecker,[c] Sandro Recchia,[a] Patrik Schmuki,[b, d, e] and Marco Altomare*[b, f]

In this work, NiCu co-catalysts on TiO$_2$ are studied for photocatalytic hydrogen evolution. NiCu co-catalyst films are deposited at room temperature by argon plasma sputtering on high aspect-ratio anodic TiO$_2$ nanotubes. To tune the Ni:Cu atomic ratio, alloys of various compositions were used as sputtering targets. Such co-catalyst films are found to be amorphous with small nanocrystalline domains. A series of parameters is investigated, i.e., i) Ni:Cu relative ratio in the sputtered films, ii) NiCu film thickness, and iii) thickness of the TiO$_2$ nanotube layers. The highest photocatalytic activity is obtained with 8 μm long TiO$_2$ nanotubes, sputter-coated with a 10 nm-thick NiCu films with a 1:1 Ni:Cu atomic ratio. This photocatalyst reaches a stable hydrogen evolution rate of 186 μL h$^{-1}$ cm$^{-2}$, 4.6 and 3 times higher than that of Ni- and Cu-TiO$_2$, respectively, demonstrating a synergistic co-catalytic effect of Ni and Cu in the alloy co-catalyst film.

## Introduction

Since Fujishima and Honda's discovery dating back to 1972 of water splitting using TiO$_2$ under UV irradiation,[1] hydrogen evolution has been the most studied photocatalytic reaction. Several semiconductors have been developed in the last decades for this purpose, but TiO$_2$ still remains the most used and investigated photocatalyst owing to its cost-effectiveness, availability, non-toxicity, stability against (photo)corrosion and suitable conduction band edge position for water reduction.[2,3] Thermodynamically, photogenerated electrons in TiO$_2$ can drive photocatalytic evolution of H$_2$. This reaction, however, is kinetically limited by the sluggish electron transfer to reactants and high charge carrier recombination in the oxide bulk. These critical features have been addressed with various strategies aimed at enhancing the photocatalytic activity of TiO$_2$. The use of nanostructured materials can limit charge carrier recombination.[2–4] In addition, improved charge carrier transfer can be achieved by decorating the surface of the photocatalyst with appropriate co-catalysts. Noble metals,[5–7] metal oxides[8–10] and carbonaceous materials[11,12] were shown to enhance the photocatalytic activity of nanostructured TiO$_2$ systems. Noble metals (e.g., Pt, Au), generally, are the most efficient co-catalysts for hydrogen evolution.[13–16] Their cost, however, has led researchers to explore cheaper alternatives with the aim of achieving comparable performance.[17–19] Earth abundant metals

[a]  M. Pinna,$^+$ Dr. D. Spanu, Prof. Dr. S. Recchia
     Department of Science and High Technology
     University of Insubria
     Via Valleggio 11
     22100 Como (Italy)
[b]  A. W. W. Wei,$^+$ Prof. Dr. P. Schmuki, Dr. M. Altomare
     Department of Materials Science WW4-LKO
     Friedrich Alexander University of Erlangen Nuremberg
     Martensstrasse 7
     91058 Erlangen (Germany)
[c]  Dr. J. Will, Dr. T. Yokosawa, Prof. Dr. E. Spiecker
     Institute of Micro- and Nanostructure Research (IMN) & Center for Nano-
     analysis and Electron Microscopy (CENEM)
     Interdisciplinary Center for Nanostructured Films (IZNF)
     Department of Materials Science and Engineering
     FAU
     Cauerstraße 3
     91058 Erlangen (Germany)
[d]  Prof. Dr. P. Schmuki
     Regional Center of Advanced Technologies and Materials
     Šlechtitelů 27
     Olomouc 78371 (Czech Republic)
[e]  Prof. Dr. P. Schmuki
     Department of Chemistry
     Faculty of Science
     King Abdulaziz University
     P.O. Box 80203
     Jeddah 21569 (Saudi Arabia)
[f]  M. Pinna,$^+$ Dr. M. Altomare
     Current affiliation:
     Photo-Catalytic Synthesis Group
     MESA + Institute for Nanotechnology
     University of Twente
     P.O. Box 217
     7500 AE Enschede (The Netherlands)
     E-mail: m.altomare@utwente.nl
[$^+$]  Equal contribution.

**ChemCatChem**

Research Article
**doi.org/10.1002/cctc.202201052**

**Chemistry
Europe**

European Chemical
Societies Publishing

such as Co,[20] Cu,[18] Ni[21] and Zn[22] have been in the spotlight. Non-noble metals, their oxides[21,23] or sulphides[24,25] were studied in combination with $TiO_2$ or other semiconductors and showed in some cases promising performance, while on average the performance of noble metals still remains higher. Bimetallic systems based on non-noble metals, such as BiCu,[26] NiFe,[27] NiCo[28] and NiCu,[29–34] were investigated owing to their intriguing optical or electronic properties compared to pure counterparts. It was shown that the enhancement in photo-catalytic activity when using bimetallic systems can be significantly higher than the activity reached using single co-catalysts. This suggests that synergistic effects arise that can improve significantly the performance of earth-abundant co-catalysts.[17,28,31,33–35] Such effects have been observed particularly for NiCu systems.[33,34,36] Typically, NiCu co-catalysts can be prepared using various techniques such as wet impregnation,[32] hydrothermal deposition,[37] chemical reduction,[30] laser ablation[29] or electrodeposition.[35] In recent own work,[33] we reported on an alternative approach for the formation of bimetallic NiCu nanoparticles. This method is based on sequential sputtering of Ni and Cu films on $TiO_2$ surfaces, followed by a thermal treatment in Ar atmosphere that induces solid-state dewetting-alloying,[33,34] i.e., the agglomeration of Ni and Cu layers forming NiCu bimetallic nanoparticles at the semiconductor surface. The particles were found to be crystalline, and featured Ni and Cu rich domains.[33] Such NiCu-$TiO_2$ systems (optimized in terms of composition and morphology) exhibited a significantly higher activity compared to the monometallic constituents (Ni-$TiO_2$ and Cu-$TiO_2$).

We follow up in the present work, adopting a more straightforward method based on direct sputtering of bimetallic alloys, from NiCu targets, for the preparation of NiCu-coated mesoporous $TiO_2$ layers. As mesoporous $TiO_2$ substrates, we use anodic $TiO_2$ nanotube (NT) layers. This strategy allows to form co-catalyst layers where Ni and Cu are already intermixed, without the need for further thermal treatments. The use of alloys as sputter targets allows also for an easy tuning of the co-catalyst composition by using a sputter target with the proper Ni and Cu ratio. Alloy targets of desired composition can in fact be easily produced since the NiCu system is fully miscible. We optimized key factors, i.e., i) NiCu relative ratio, ii) thickness of NiCu layer and iii) thickness of $TiO_2$ NTs, to maximize the photocatalytic $H_2$ evolution performance. The highest hydrogen evolution rate (186 $\mu L\,h^{-1}\,cm^{-2}$, 4.6 and 3 times higher than that of Ni– and Cu–$TiO_2$, respectively) was obtained using ~8 $\mu m$-long $TiO_2$ NTs decorated with a 10 nm-thick NiCu co-catalyst layer with 1:1 at.% NiCu composition. Our results confirm that bimetallic systems such as NiCu layers can provide a synergistic co-catalytic effect for $H_2$ evolution. Moreover, the NiCu co-catalyst is not required to be crystalline to provide a photocatalytic improvement, as the NiCu sputtered films used in this work are of amorphous nature. This simple methodology opens for the screening of new earth abundant co-catalysts, for example by depositing multinary systems on mesoporous photocatalytic surfaces.

## Results and Discussion

In the present work, high aspect-ratio titanium dioxide nanotube arrays were used as photocatalytic active layers. $TiO_2$ NTs were grown by anodizing a Ti foil in an ethylene glycol solution to produce several micrometer-thick layers. In Figure 1a–b it is possible to observe the morphological features of the formed tubes, namely, a pore top opening of ~70 nm and a tube length of ~6.5 $\mu m$. This NT length was chosen for preliminary experiments as it is reported in literature that it provides the highest photocatalytic activity due to optimized light absorption and charge carrier separation.[38]

After anodization, the materials were annealed at 450 °C for 1 h to crystallize the amorphous $TiO_2$. Diffraction peaks were attributed to either anatase $TiO_2$ or Ti metal (substrate) as reported in Figure 1c and *Table S1* (Supporting Information). No rutile peaks were detected meaning that annealing under these conditions converts amorphous $TiO_2$ to pure anatase.

The crystalline $TiO_2$ NTs were subsequently coated by plasma sputtering with 10 nm-thick metal films using pure nickel, pure copper, and their alloys with three different NiCu ratios (25:75, 50:50 and 75:25) as sputter target materials. A scheme of the photocatalyst preparation is provided in *Figure S1*. The alloys are named as 25Ni75Cu, 50Ni50Cu and 75Ni25Cu according to their nominal composition. The morphology of NiCu-decorated systems are shown in Figure 2a–f.

The morphology of the co-catalyst layers varies depending on the composition. Co-catalysts formed by sputtering from Cu-rich targets are characterized by the presence of isolated particles with an estimated size of ~20–35 nm, whereas Ni-rich coatings appear as dense films featuring a nanoparticulate
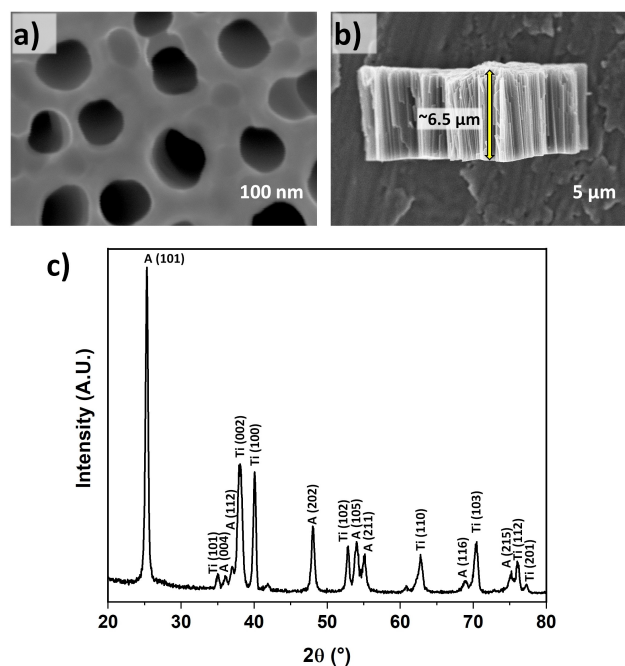


**Figure 1.** a) SEM top and b) cross-section view of pristine $TiO_2$ NTs. c) X-ray diffraction pattern of pristine $TiO_2$.

**ChemCatChem**

Research Article
doi.org/10.1002/cctc.202201052

**Chemistry Europe**
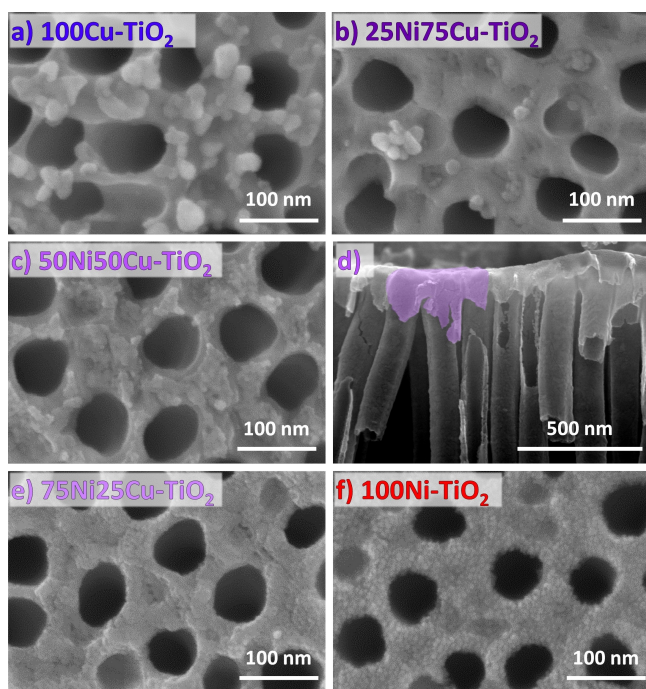European Chemical
Societies Publishing

**Figure 2.** SEM top views of $TiO_2$ NTs after the deposition of a) pure Cu, f) pure Ni and b), c), e) NiCu alloys with different compositions (nominal thickness of 10 nm for all the samples). d) SEM cross section view of 50Ni50Cu–$TiO_2$ revealing the alloy penetration in the nanostructures.

the XRD patterns may be due to the low co-catalyst loading (10 nm-thick NiCu layer), or to the nature of such layers (sputtered at room temperature) which were found to be nanocrystalline, as discussed along with TEM results below.

The Ni:Cu composition ratio and oxidation state of Ni and Cu were investigated by XPS. This study was carried out using Ni-, Cu- and NiCu-sputtered layers (10 nm-thick) on Si wafers. For simplicity, we used Si substrates to avoid the undefined top morphology of nanotubes and their large oxygen content. On the contrary, Si wafers are atomically flat and carry only a very thin (ca. 1–2 nm thick) native surface oxide layer. Figure 3a shows that the surface composition of the sputtered co-catalyst layers changes accordingly to the target used for deposition. Only minor deviations from the nominal target compositions were observed. These small discrepancies may be ascribed to the different sputter yield of Ni and Cu.[39]

The XPS depth profile analysis for the 50Ni50Cu layer (Figure 3b and *Table S2*) reveals that the outermost NiCu region features a higher oxygen content and a higher Cu concentration than in depth. Sputtering to a depth of 3 or 6 nm, instead, shows i) an almost 1:1 Ni:Cu atomic ratio, that is in line with the sputter target composition, and ii) a much lower oxygen content (ca. a half of that found at the surface). The large content of oxygen in the surface can be explained assuming surface oxidation of the NiCu layers when exposed to air. The presence of oxygen in depth may not be due to sample exposure to the environment but suggests some oxygen incorporation during sputtering (discussed below). As for the variation of the Ni:Cu ratio, the different sputtering yield for Ni and Cu can be the cause of the inhomogeneity along the depth of the layer.

High resolution XPS spectra (reported in Figures 4 and 5) were recorded for Cu2p, Ni2p and O1s, and were analyzed to determine the oxidation state of Cu and Ni in the sputtered layers. Regarding Cu, it is possible to observe for all Cu-containing samples (Figures 4a–d) the presence of both metallic Cu (932.6 eV), and oxidized Cu species (see CuO and $Cu(OH)_2$

texture (diameter of the nanoparticles $< 10$ nm). Besides, at the surface of the photocatalysts it is possible to notice the penetration of the sputtered layers inside the nanotubular structure to a depth of a few hundred nanometers (Figure 2d). Thus, only the outermost part of the NTs is coated by the sputtered co-catalyst.

Although clearly visible by SEM observations, the presence of Ni and Cu species was not detected by X-Ray diffraction measurements (Figure S2). The absence of Ni and Cu signals in
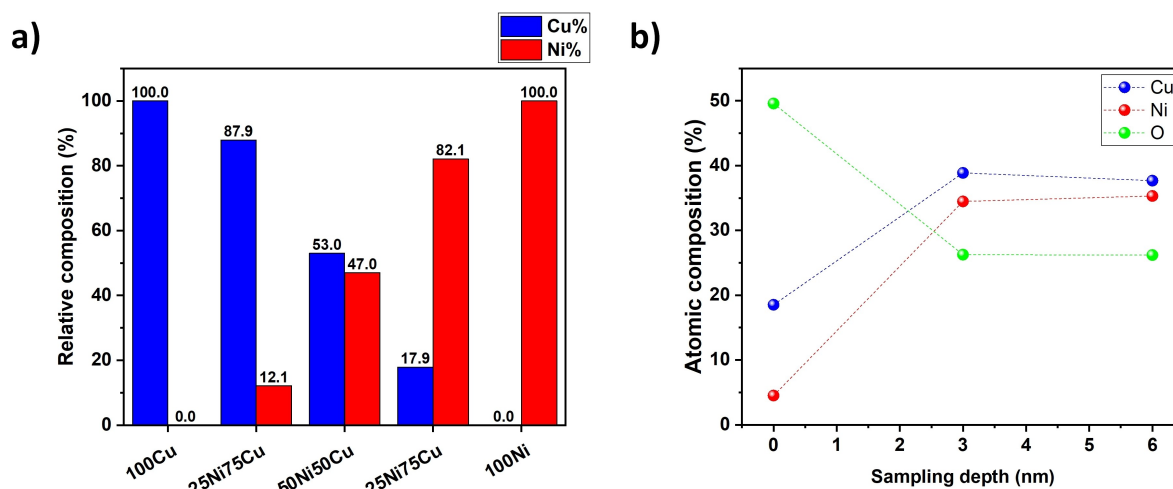


**Figure 3.** a) Ni and Cu relative content obtained by XPS analysis at a sampling depth of 3 nm for Ni, Cu and NiCu alloys (10 nm-thick layer) sputtered on Si wafer. b) XPS depth profile analysis for 50Ni50Cu alloy (10 nm-thick layer) sputtered on Si wafer.
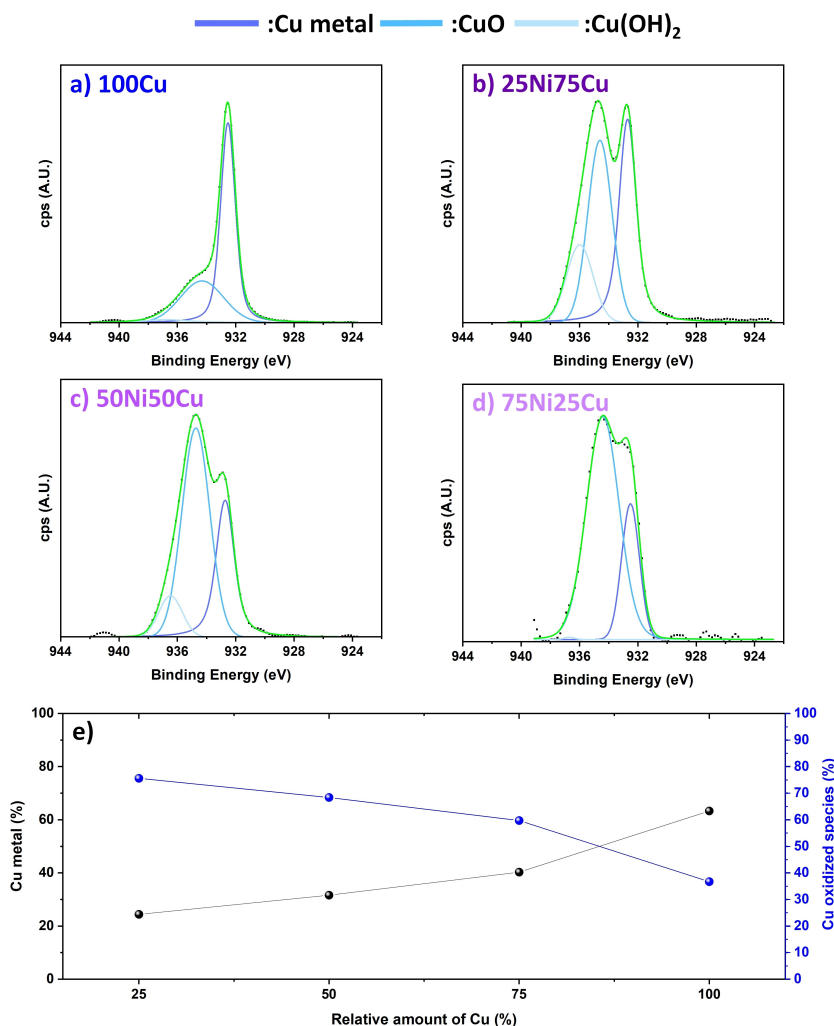
**ChemCatChem**

Research Article
doi.org/10.1002/cctc.202201052

Chemistry
Europe

European Chemical
Societies Publishing

**Figure 4.** a-d) High resolution XPS spectra in the Cu2p region for all Cu-containing NiCu layers. e) Relative content of metal and oxidized Cu (sum of CuO and Cu(OH)$_2$ species) by varying the composition of the NiCu layers.

peaks at higher binding energies). These species differ in their relative content when varying the composition of the sputtered layer: the fraction of metallic Cu phase decreases as the Ni amount in the alloy increases, i.e., leading to the presence of larger amounts of oxidized Cu species in Ni-rich alloys. The relative content of Cu(0) ranges from 63.3% in 100Cu to 29.2% in 75Ni25Cu (see Figure 4e and Table S3). Analogously, also the speciation of Ni is affected by the composition of the alloy: the peak of Ni(0) at 852.6 eV is visible only for Cu-rich alloys, i.e., 25Ni75Cu and 50Ni50Cu (see Figures 5b *and 5c*). Such peak is not observed for other Ni-rich samples (100Ni and 75Ni25Cu, see Figures 5a and 5d). In the case of Ni, the relative content of metallic phase is much lower than that of oxidized Ni species. The content of oxidized Ni species (sum of NiO (853.9 eV) and Ni(OH)$_2$ (855.7 eV)) ranges from 2.3% in 25Ni75Cu to 0% in 100Ni and 75NiCu (Figure 5e *and Table S3*). The presence of oxidized Ni and Cu species is also confirmed by O1s signals (Figure S3): the peak at 529.5 eV (present only in Ni-rich samples) is associated to the presence of NiO[40] whereas the peak at 530.3 eV (present only in Cu-rich samples) is related to

the presence of CuO.[41] A second peak at 531.3-531.6 eV is present in all the samples and may be ascribed to the presence of defects in the metal oxide layer.[42] Finally, high resolution XPS measurements taken for Cu2p and Ni2p (Figure S4) at different depths (by Ar sputter-etching) indicate that not only the surface, but the entire layer is partially oxidized as practically no Cu and Ni metal phases are present in the inner regions of the layer. These results are well in line with data shown in Figure 3b and can be explained by considering the relatively high background pressure used during sputtering (10$^{-2}$ mbar), i.e., traces of oxygen may be incorporated during film deposition. The incorporation of oxygen during deposition may also account for the fact that Cu-rich layers contain lower amounts of oxidized phases for both Cu and Ni (*Figure S3*). In general, the larger the Cu content, the lower the amount of oxygen incorporated in the sputtered layer. Conversely, the content of oxidized phases increases with increasing the atomic fraction of Ni in the NiCu layer.

Electron microscopy in combination with energy dispersive X-ray spectroscopy (EDXS) was employed to shed light on
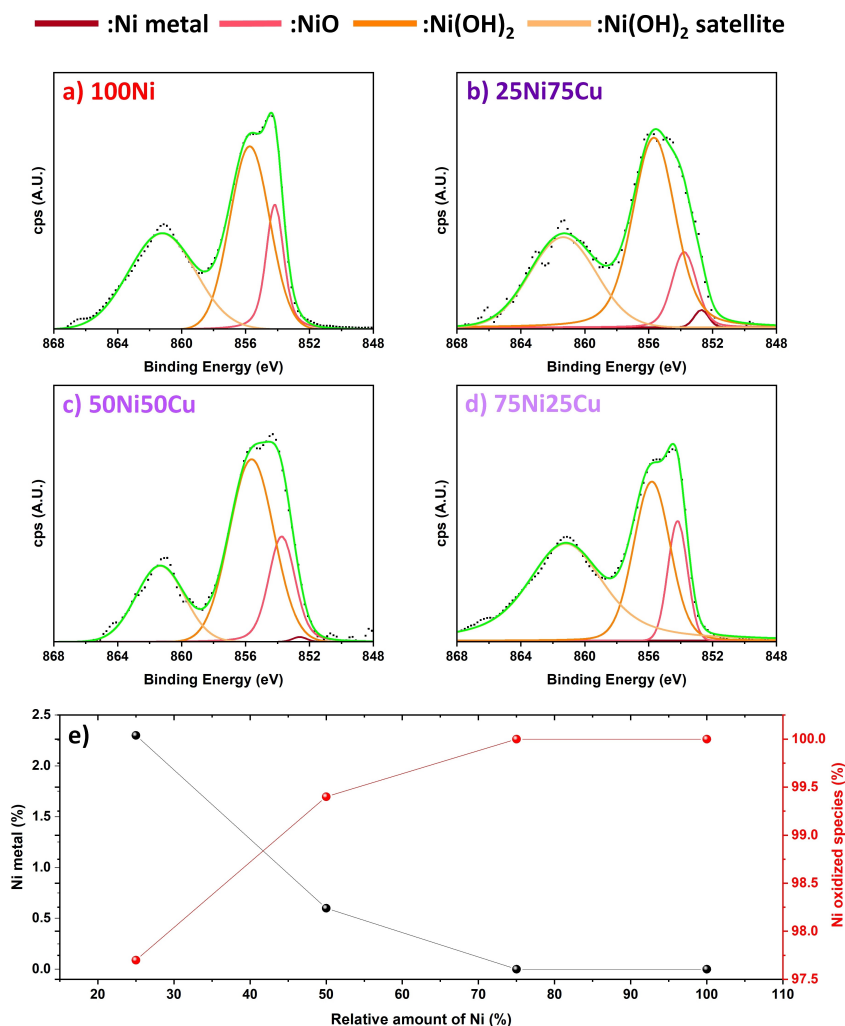
**ChemCatChem**

Research Article
doi.org/10.1002/cctc.202201052

**Chemistry
Europe**

European Chemical
Societies Publishing

**Figure 5.** a-d) High resolution XPS spectra in the Ni2p region for all Ni-containing NiCu layers. e) Relative content of metal and oxidized Ni (sum of NiO and Ni(OH)$_2$ species) by varying the composition of the NiCu layers.

composition, structure, and morphology of a 50Ni50Cu atop the TiO$_2$ nanotubes. An EDXS map of the nanotube top is shown in Figure 6a. The corresponding line profiles (Figure 6b) along the arrow indicated in Figure 6a confirm the nominal composition in line with the XPS data of Figure 3. In addition, the NiCu signal decreases towards the bulk within the outermost ~0.6 μm. Scanning transmission electron microscopy (STEM) of the film as compiled in Figure 6c-d reveal NiCu island with lateral as well as vertical dimensions of a few ten nm, confirming what observed in the SEM images. Moreover, nanocrystalline domains are visible in high-resolution STEM bright field (BF) images (Figure 6d).

To confirm the nanocrystalline nature of the film and the anatase phase of the nanotubes, selected area electron diffraction (SAED) is performed on the bulk and on the top part (Figure 6e) of a nanotube in cross-section. The corresponding diffraction patterns are radially integrated and compared with the theoretical peak positions of anatase and Cu. The compiled data in Figure 6f confirm i) the anatase phase of the nanotubes (top and bulk) and ii) the nanocrystalline nature of the NiCu

film. The 111 reflection of Cu (which is close to the 111 reflection of Ni) appears as a weak and broad hump in the SAED pattern taken at the top, which confirms i) the presence of crystalline Cu(Ni) species and ii) the nanocrystalline character of the films. Note that peak broadening can originate from both a finite crystalline domain size and local variations in the NiCu composition.

The NiCu-coated photocatalyst layers were characterized in view of their photocatalytic performance. Preliminary photocatalytic hydrogen evolution tests were conducted under UV light (365 nm) for a total illumination time of 4 hours in a 20% EtOH–H$_2$O using NiCu–TiO$_2$ systems. Coating the NiCu co-catalyst only on the top of the nanotube structure leaves free TiO$_2$ surface inside the nanotubes where the hole mediated oxidation of ethanol likely takes place, while hydrogen evolution takes place at the NiCu surface. A sketch of the proposed H$_2$ evolution mechanism by ethanol photocatalytic reforming on NiCu–TiO$_2$ is provided in the SI, Figure S5.

We tested first TiO$_2$ nanotubes sputter-coated with 10 nm-thick co-catalyst layers of different composition (samples shown
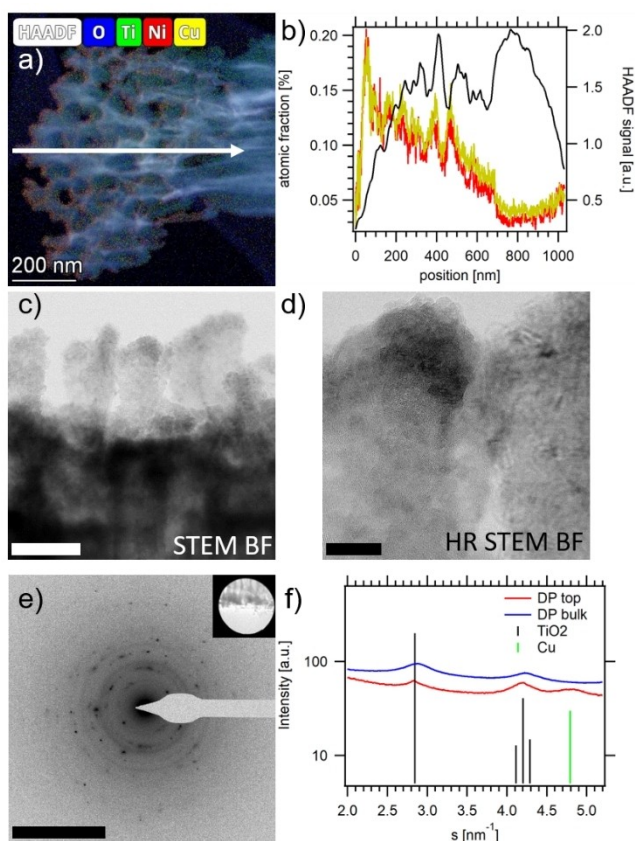
**Figure 6.** a) EDXS map of the top part of a nanotube. b) Line profiles along the white arrow drawn in a). c) STEM bright field (BF) image of a top part of a nanotube in cross-section (scale bar 50 nm). d) High-resolution BF image of a top part of a nanotube (scale bar 10 nm). e) Selected area diffraction pattern (SAED) of the nanotube top as depicted in the inset (scale bar 10 nm$^{-1}$). f) Radially integrated SAED patterns comparing the top part of the nanotube to its bulk.

in Figure 2). The results of these experiments are summarized in Figure 7. The data reveal that undecorated $TiO_2$ NTs, as expected, show a negligible photocatalytic $H_2$ generation
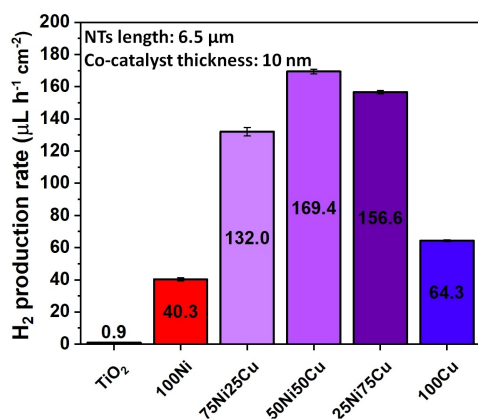
$(0.9\ \mu L\,h^{-1}\,cm^{-2})$. Differently, $TiO_2$ NTs coated with pure Cu and Ni layers exhibit an improved $H_2$ production rate $(64.3\ \mu L\,h^{-1}\,cm^{-2}$ and $40.3\ \mu L\,h^{-1}\,cm^{-2}$, respectively). However, highest photocatalytic $H_2$ evolution rates are always obtained when using NiCu-decorated $TiO_2$ NTs, regardless of the NiCu relative composition. The samples 25Ni75Cu-, 50Ni50Cu- and 75Ni25Cu-$TiO_2$ provide a clearly higher photocatalytic efficiency compared to pure Ni- or Cu-modified $TiO_2$ (using the same total metal loading). 50Ni50Cu-$TiO_2$ is the most performing photocatalyst, showing an $H_2$ generation rate of $169.4\ \mu L\,h^{-1}\,cm^{-2}$, i.e., around 190 times higher than pristine $TiO_2$ and ~2.6 and ~4.2 times higher than that of 100Cu– and 100Ni–$TiO_2$, respectively. It is interesting to note that the activity observed for any bimetallic NiCu system is substantially higher than the sum of the activity of pure Ni and Cu co-catalysts layers. This suggests that the bimetallic systems provide synergistic effects, as also proposed in previous work.[33,43,44] Electronic interactions of Ni atoms with neighboring Cu atoms allow to modulate (reduce) the binding energy of protons on active sites, which may enhance the kinetics of $H_2$ evolution.[43,45,46] We performed linear sweep voltammetry (LSV) experiments to characterize the electrochemical hydrogen evolution reaction (HER) activity of bimetallic NiCu films vs. monometallic Ni or Cu films. For this, Ni, Cu and NiCu films (50 nm-thick) were sputter-coated on electrically conductive fluorine-doped tin oxide (FTO) slides and tested as working electrodes for HER in a 3-electrode electrochemical cell. Results (*Figure S6*) are discussed in the SI. Briefly, the electrochemical HER trend (Ni > NiCu > Cu), in terms of overpotential required to drive HER at -10 mA cm$^{-2}$, differs from that observed in the photocatalytic $H_2$ evolution experiments, i.e., NiCu > Cu > Ni (Figure 7). However, when comparing ("open circuit") photocatalytic results with electrochemical HER data (polarization curves) one should carefully consider the different "exit energy" of $TiO_2$ conduction band electrons (i.e., the potential of the CB minimum) vs. the applied external electrical bias.

Regarding the presence of oxidized Ni and Cu species in the co-catalyst film as shown by XPS results (above, Figures 4 and 5): it is worth to point out that in previous own work[34] on Ni-, Cu-, and NiCu nanoparticle-modified $TiO_2$ we demonstrated that, under illumination, oxidized Ni and Cu species such as native oxides at the co-catalyst surface are promptly reduced to a metallic phase. Reduction of such oxidized Ni and Cu species can be driven by photo-promoted CB electrons. Thus, it is possible that also the oxidized Ni and Cu species present in the herein studied NiCu films undergo reduction to a NiCu metal phase under illumination and in the presence of ethanol as hole-scavenger.

Additionally, theoretical calculations shows that the work function of NiCu increases from 4.65 eV (pure Cu) up to 5.11 (pure Ni) as nickel content increases, and this provides a higher Schottky barrier that may grant a better charge carrier separation at the semiconductor/metal interface.[47–50]

Finally, the NiCu co-catalyst films provide a significant $H_2$ evolution enhancement despite being mainly amorphous with nm-sized crystalline domains. This indicates that a high degree of crystallinity of the co-catalyst is not a strict requirement to



**Figure 7.** Hydrogen evolution rates obtained by varying the composition of the co-catalyst layer.

**ChemCatChem**

Research Article
doi.org/10.1002/cctc.202201052

**Chemistry Europe**
European Chemical
Societies Publishing

mediate electron transfer and proton reduction. Similar observations were made in a few recent articles studying amorphous metal, oxide, or sulfide co-catalysts.[51–54]

After determining the optimal Ni:Cu ratio, parameters such as the co-catalyst layer thickness and the length of the $TiO_2$ NTs were investigated. Firstly, 6.5 μm long $TiO_2$ NTs were coated with 50Ni50Cu alloy layers of different nominal thickness obtained by varying the sputtering time. The morphologies of the resulting materials are shown in Figures 8a-f. When depositing NiCu layers with nominal thickness < 5 nm, no structural change of the NT top surface can be appreciated by SEM (Figures 8a–c). Thicker layers (10, 15 and 20 nm) are instead clearly visible and feature a less smooth and uniform appearance with increasing the layer thickness (Figures 8d–f). Interestingly, the samples decorated with 15 and 20 nm thick layers are characterized by the presence of cubic shaped nanoparticles. This might be due to the formation of CuO crystals.[55,56] Moreover, thick NiCu films partially clog the top opening of the NTs.

These samples were tested in view of their photocatalytic activity towards hydrogen evolution. The results are shown in Figure 9a. A marked increase in photocatalytic performance was observed for all NiCu-decorated samples reaching an optimal performance with the 10 nm-thick layer. This can be considered the best compromise in terms of activity versus amount of co-catalyst. Thicker layers (15 and 20 nm) resulted in a decreased photocatalytic activity probably due to the excessive coverage of the $TiO_2$ surface which may cause i) a reduction of the available surface area for photocatalysis due to the clogging of the tube opening and ii) shadowing effects leading to a lower photon flux reaching the $TiO_2$ layer.

Finally, we explored the effect of the length of $TiO_2$ NTs on the photocatalytic $H_2$ evolution performance of (10 nm) 50Ni50Cu-$TiO_2$ (Figure 9b). Nanotubes with different thicknesses were synthetized by varying the anodization time. The results, summarized in Figure 9b, clearly show that an increase in nanotubes length up to 6.5 μm results in an enhanced photocatalytic activity. This is because thicker nanotubes layers offer improved light absorption.[38] In line with literature data,

increasing the length of nanotubes above 6–8 μm does not improve the photocatalytic activity further. Hence, one can conclude that thicker nanotube layers do not offer improved optical absorption and charge collection efficiency.[38] The optimal nanotube length is thus be 8.5 μm, providing a hydrogen evolution rate of 186.3 μL h$^{-1}$ cm$^{-2}$, which corresponds to an estimated apparent quantum yield of 1.39% (see details on AQY estimation in the SI).

Once identified the most active photocatalyst by tuning the composition of the sputtered co-catalyst layer (Ni:Cu ratio ~1), its thickness (10 nm) and the thickness of the $TiO_2$ NT layer (8.5 μm), repeated tests were conducted using the same sample (Figure 9c). In these consecutive tests, only minor variations in the generated $H_2$ amount were observed (with no clear trend), indicating an average $H_2$ evolution rate of 203 ± 19 μL h$^{-1}$ cm$^{-2}$ with no significant activity decay taking place after five photocatalytic tests.

## Conclusions

We demonstrated the preparation of a noble metal-free photocatalyst for hydrogen evolution by sputtering NiCu alloy films on the surface of mesoporous $TiO_2$ layers (high aspect ratio $TiO_2$ nanotube layers). We investigated the photocatalyst activity towards hydrogen evolution by screening the effect of i) the Ni:Cu relative ratio, ii) the NiCu film thickness and iii) the $TiO_2$ nanotube length. We found that 10 nm-thick NiCu layers sputtered from 50Cu:50Ni targets on ~8.5 μm-thick $TiO_2$ nanotube layers provide a highest efficiency for hydrogen evolution, i.e., 186.3 μL h$^{-1}$ cm$^{-2}$, which is 200 times higher than pristine $TiO_2$ nanotubes (0.6 μL h$^{-1}$ cm$^{-2}$), and 4.6 (40.3 μL h$^{-1}$ cm$^{-2}$) and 3 (64.3 μL h$^{-1}$ cm$^{-2}$) times higher than pure Ni- and Cu-$TiO_2$, respectively. The activity enhancement observed for bimetallic NiCu co-catalysts is substantially higher than the sum of the activity of pure Ni and Cu co-catalysts. This suggests that the bimetallic layers provide a synergistic effects, i.e., electronic interactions of Ni atoms with neighboring Cu atoms allow to modulate (reduce) the binding energy of protons on active
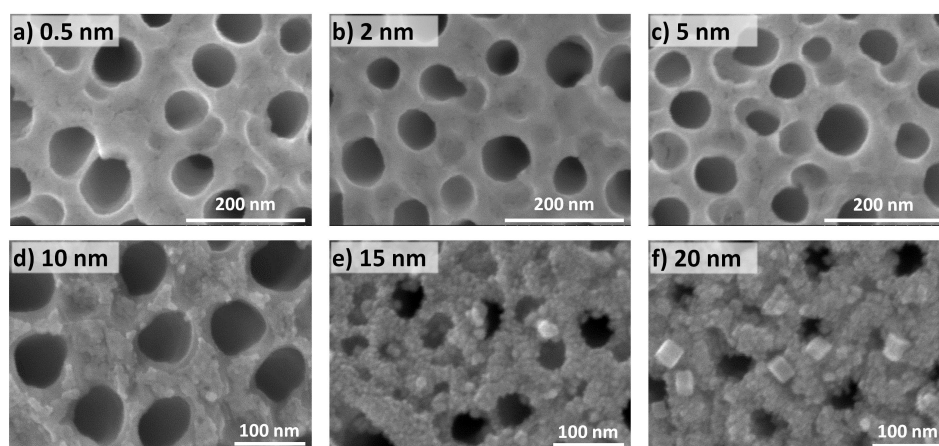


**Figure 8.** SEM top view images of 50Ni50Cu-$TiO_2$ samples (6.5 μm long $TiO_2$ nanotubes) coated with alloy layers of different thickness.

**ChemCatChem**

Research Article
doi.org/10.1002/cctc.202201052

**Chemistry
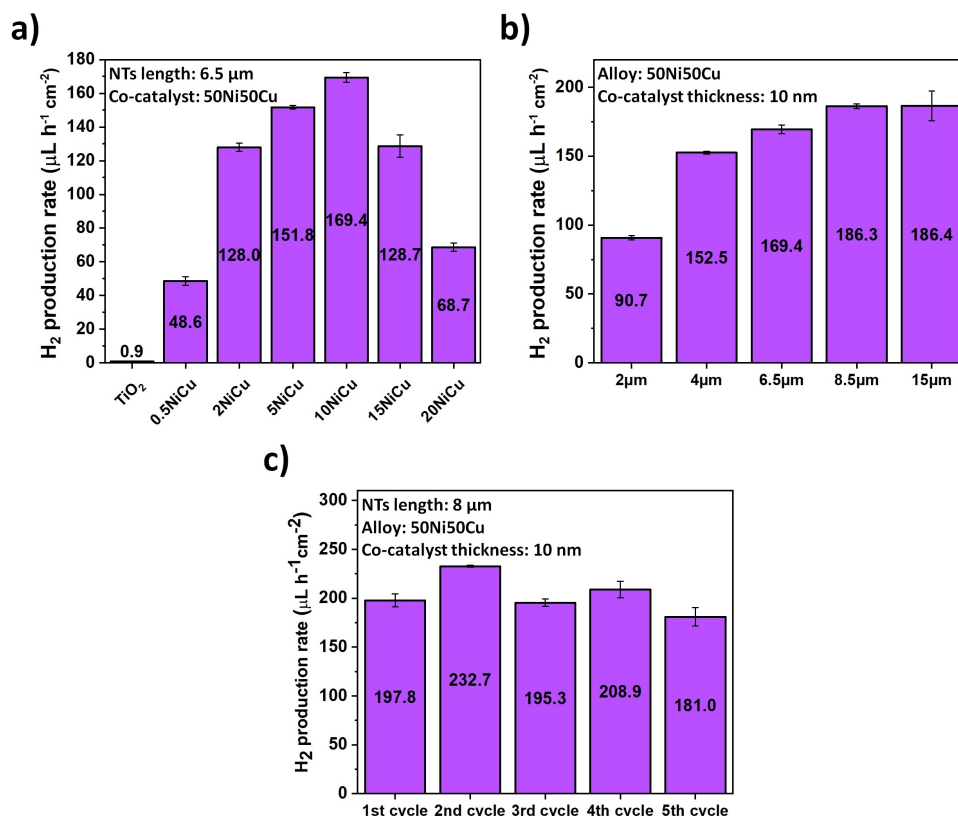Europe**
European Chemical
Societies Publishing

**Figure 9.** a-c) Hydrogen evolution rate obtained by varying different features of the photocatalyst a) the thickness of 50Ni50Cu co-catalyst layer; b) the TiO$_2$ nanotube layer thickness (decorated with 50Ni50Cu, 10 nm); c) Repeated tests for the optimal photocatalyst (10 nm 50Ni50Cu on 8 μm thick NT layers).

sites, which may enhance the kinetics of H$_2$ evolution. In future work, we will address the stability of Ni and Cu species under intermittent illumination (light on-off cycles).

## Experimental

### Fabrication of the TiO$_2$ nanotubes array and thermal treatment

Ti foils (Advent Research Materials, 0.125 mm thickness, 99.6+ purity) were degreased by sonication in acetone, ethanol, ultrapure water and were then dried under a N$_2$ stream. Then, the cleaned Ti foils were anodized in an ethylene glycol electrolyte with a NH$_4$F concentration of 0.15 M and 3 vol.% H$_2$O content. For the anodic growth, a two-electrode configuration was used, where the Ti foil (15 mm×15 mm) and a Pt sheet were used as working and counter electrode, respectively. We used a bottom mount electrochemical cell with an O-ring diameter of 1 cm. The choice of using anodic TiO$_2$ nanotube layers was made as their morphology can be tuned by controlling simple experimental parameters and because of their high surface area. The anodization experiments were carried out by applying a potential of 60 V using a DC power supply (VLP 2403 Volcraft). Anodization time was varied to tune the thickness of the nanotube layers. To obtain 6.5 μm-long nanotubes, a time of 17 minutes was used. Additional information on times used for anodization can be found in *Table S4* (Supporting Information). After anodization, the samples were rinsed and soaked in ethanol overnight (to remove the residual adsorbed electrolyte), subse-

quently they were dried in a N$_2$ stream. Finally, the amorphous TiO$_2$ nanotubes were annealed at 450 °C for 1 h in air to crystallize the oxide into anatase phase.

### Sputter deposition of Ni, Cu and NiCu

In order to coat the outermost surface of the nanotubes arrays, a plasma sputter-coater (EM SCD 500, Leica) was used to sputter Cu, Ni and NiCu alloy layers using the following targets: Cu (99.60 at.% pure, Baltic praeparation e.K), Ni (99.98 at.% pure), 25Ni75Cu (25% Ni-75%Cu, at.%), 50Ni50Cu (50%Ni-50%Cu, at.%) and 75Ni25Cu (75%Ni-25%Cu, at.%). Besides Cu, all sputter targets were provided by Hauner Metallische Werkstoffe, Germany. In any case the applied sputtering current was set to 16 mA and the pressure of the sputtering chamber was set at 10$^{-2}$ mbar of Ar. The amount of sputtered metal, i.e., the nominal thickness of the co-catalyst film, was in situ determined by an automated quartz crystal film-thickness sensor.

### Characterization of materials

To examine the crystallographic properties of the materials, X-ray diffraction (XRD) was performed using a X'pert Philips MPD (equipped with a Panalytical X'celerator detector), using graphite monochromized Cu Kα radiation (wavelength 1.54056 Å). The measurements were carried out with the following parameters: step size 0.03°; time per step 2 s; scan rate (continuous) 0.015° s$^{-1}$. A field-emission scanning electron microscope (FE-SEM, Hitachi S4800) and a transmission electron microscope (TEM TITAN 60–300, FEI, USA) were used to characterize the morphology of the

**ChemCatChem**

Research Article
doi.org/10.1002/cctc.202201052

**Chemistry
Europe**
European Chemical
Societies Publishing

photocatalysts. The double corrected TEM was operated at 300 kV. Electron dispersive X-ray spectroscopy maps were taken with a Super-X detector and bright filed scanning TEM (STEM) images were taken with a collection angle of 6 mrad. The composition of the samples was analyzed by X-ray photoelectron spectroscopy (XPS, PHI 5600, US) and peak positions were calibrated with respect to the C1s peak at 285 eV. The fitting of the XPS peaks was performed using Origin 2018 software (OriginLab, Northampton). The XPS sputter rate was calibrated by sputtering through thermal $SiO_2$ layers of known thickness on Si wafers.

### Electrochemical hydrogen evolution experiments

Experiments were conducted with a three-electrode cell configuration using a Ag/AgCl electrode (3 M KCl) as reference electrode, platinized titania as counter electrode and aqueous 0.5 M $Na_2SO_4$ solution as electrolyte (pH ~6.3). Ni, Cu and NiCu films (50 nm-thick) were sputter-coated on electrically conductive fluorine-doped tin oxide (FTO) slides and tested as working electrodes for the hydrogen evolution reaction (HER). The HER performance of the samples was evaluated in terms of overpotential at geometric current density of $-10\ mA\,cm^{-2}$. Potentials are referred to the reversible hydrogen electrode (RHE) and are iR corrected.

### Photocatalytic experiments

Photocatalytic measurements for $H_2$ generation were carried out by irradiating the photocatalyst layers in a 20% ethanol-water solution (ethanol was used as a hole-scavenger) in a quartz tube sealed with a gas-tight cap for a total of 4 hours. As light source, we used a LED UV light (Opsytec, 365 nm, beam size 0.785 $cm^2$) with a power of 100 $mW\,cm^{-2}$. The ethanol-water solution and the cell headspace (volume 5.12 mL) were purged with $N_2$ gas for 15 minutes prior to the $H_2$ evolution tests.

The amount of produced $H_2$ was measured by using a gas chromatograph (GCMSQO2010SE, Shimadzu) equipped with a thermal conductivity detector and a Restek micropacked Shin Carbon ST column (2 m×0.53 mm). Recycling tests were performed as following: at the end of a 4 h photocatalytic test, the photocatalyst was rinsed and placedin the quartz tube in a fresh 20% EtOH-$H_2O$ solution and was again irradiated with UV light (365 nm) for 4 h.

## *Acknowledgements*

## *Conflict of Interest*

The authors declare no conflict of interest.

## Data Availability Statement

The data that support the findings of this study are available from the corresponding author upon reasonable request.

[1] A. Fujishima, K. Honda, *Nature* **1972**, *238*, 37–38.
[2] P. Roy, S. Berger, P. Schmuki, *Angew. Chem. Int. Ed.* **2011**, *50*, 2904–2939; *Angew. Chem.* **2011**, *123*, 2956–2995.
[3] K. Lee, A. Mazare, P. Schmuki, *Chem. Rev.* **2014**, *114*, 9385–9454.
[4] F. Riboni, N. T. Nguyen, S. So, P. Schmuki, *Nanoscale Horiz.* **2016**, *1*, 445–466.
[5] A. Naldoni, M. D'Arienzo, M. Altomare, M. Marelli, R. Scotti, F. Morazzoni, E. Selli, V. Dal Santo, *Appl. Catal. B* **2013**, *130–131*, 239–248.
[6] M. Murdoch, G. I. N. Waterhouse, M. A. Nadeem, J. B. Metson, M. A. Keane, R. F. Howe, J. Llorca, H. Idriss, *Nat. Chem.* **2011**, *3*, 489–492.
[7] D. Spanu, A. Bestetti, H. Hildebrand, P. Schmuki, M. Altomare, S. Recchia, *Photochem. Photobiol. Sci.* **2019**, *18*, 1046–1055.
[8] İ. Ç. Davaslıoğlu, K. Volkan Özdokur, S. Koçak, Ç. Çırak, B. Çağlar, B. B. Çırak, F. Nil Ertaş, *J. Mol. Struct.* **2021**, *1241*, DOI 10.1016/j.molstruc.2021.130673.
[9] W. H. Lee, C. W. Lai, S. B. Abd Hamid, *Materials* **2015**, *8*, 5702–5714.
[10] S. Ozkan, G. Cha, A. Mazare, P. Schmuki, *Nanotechnology* **2018**, *29*, DOI 10.1088/1361-6528/aab062.
[11] Q. Wang, J. Huang, H. Sun, K. Q. Zhang, Y. Lai, *Nanoscale* **2017**, *9*, 16046–16058.
[12] M. Pinna, G. Binda, M. Altomare, M. Marelli, C. Dossi, D. Monticelli, D. Spanu, S. Recchia, *Catalysts* **2021**, *11*, DOI 10.3390/catal11091048.
[13] S. Xu, J. Ng, X. Zhang, H. Bai, D. D. Sun, *Int. J. Hydrogen Energy* **2010**, *35*, 5254–5261.
[14] M. Jung, J. N. Hart, J. Scott, Y. H. Ng, Y. Jiang, R. Amal, *Appl. Catal. A* **2016**, *521*, 190–201.
[15] H. J. Choi, M. Kang, *Int. J. Hydrogen Energy* **2007**, *32*, 3841–3848.
[16] L. S. Yoong, F. K. Chong, B. K. Dutta, *Energy* **2009**, *34*, 1652–1661.
[17] H. Tian, S. Z. Kang, X. Li, L. Qin, M. Ji, J. Mu, *Sol. Energy Mater. Sol. Cells* **2015**, *134*, 309–317.
[18] S. Zhang, B. Peng, S. Yang, H. Wang, H. Yu, Y. Fang, F. Peng, *Int. J. Hydrogen Energy* **2015**, *40*, 303–310.
[19] C. Xia, T. Hong Chuong Nguyen, X. Cuong Nguyen, S. Young Kim, D. L. T. Nguyen, P. Raizada, P. Singh, V. H. Nguyen, C. Chien Nguyen, V. Chinh Hoang, Q. van Le, *Fuel* **2022**, *307*, DOI 10.1016/j.fuel.2021.121745.
[20] P. D. Tran, L. Xi, S. K. Batabyal, L. H. Wong, J. Barber, J. S. Chye Loo, *Phys. Chem. Chem. Phys.* **2012**, *14*, 11596–11599.
[21] M. T. Uddin, Y. Nicolas, C. Olivier, W. Jaegermann, N. Rockstroh, H. Junge, T. Toupance, *Phys. Chem. Chem. Phys.* **2017**, *19*, 19279–19288.
[22] S. Guo, S. Han, H. Mao, S. Dong, C. Wu, L. Jia, B. Chi, J. Pu, J. Li, *J. Power Sources* **2014**, *245*, 979–985.
[23] M. Alhaddad, A. A. Ismail, Y. G. Alghamdi, N. D. Al-Khathami, R. M. Mohamed, *Opt. Mater. (Amsterdam, Neth.)* **2022**, *131*, 112643.
[24] P. Wang, S. Xu, F. Chen, H. Yu, *Chin. J. Catal.* **2019**, *40*, 343–351.
[25] T. R. Kuo, H. J. Liao, Y. T. Chen, C. Y. Wei, C. C. Chang, Y. C. Chen, Y. H. Chang, J. C. Lin, Y. C. Lee, C. Y. Wen, S. S. Li, K. H. Lin, D. Y. Wang, *Green Chem.* **2018**, *20*, 1640–1647.
[26] Z. Khazaee, A. R. Mahjoub, A. H. Cheshme Khavar, *Appl. Catal. B* **2021**, *297*, DOI 10.1016/j.apcatb.2021.120480.
[27] B. Tudu, N. Nalajala, K. Prabhakar Reddy, P. Saikia, C. S. Gopinath, *ACS Sustainable Chem. Eng.* **2021**, *9*, 13915–13925.
[28] P. D. Tran, L. Xi, S. K. Batabyal, L. H. Wong, J. Barber, J. S. Chye Loo, *Phys. Chem. Chem. Phys.* **2012**, *14*, 11596–11599.
[29] Z. Lin, J. Li, L. Li, L. Yu, W. Li, G. Yang, *J. Mater. Chem. A* **2017**, *5*, 773–781.
[30] Y. Yamada, S. Shikano, S. Fukuzumi, *RSC Adv.* **2015**, *5*, 44912–44919.
[31] B. Seemala, C. M. Cai, C. E. Wyman, P. Christopher, *ACS Catal.* **2017**, *7*, 4070–4082.
[32] N. Riaz, F. K. Chong, Z. B. Man, R. Sarwar, U. Farooq, A. Khan, M. S. Khan, *RSC Adv.* **2016**, *6*, 55650–55665.
[33] D. Spanu, S. Recchia, S. Mohajernia, O. Tomanec, Š. Kment, R. Zboril, P. Schmuki, M. Altomare, *ACS Catal.* **2018**, *8*, 5298–5305.

**ChemCatChem**

Research Article
**doi.org/10.1002/cctc.202201052**

**Chemistry
Europe**
European Chemical
Societies Publishing

[34] D. Spanu, A. Minguzzi, S. Recchia, F. Shahvardanfard, O. Tomanec, R. Zboril, P. Schmuki, P. Ghigna, M. Altomare, *ACS Catal.* **2020**, *10*, 8293–8302.

[35] X. Li, J. Yao, F. Liu, H. He, M. Zhou, N. Mao, P. Xiao, Y. Zhang, *Sens. Actuators B* **2013**, *181*, 501–508.

[36] M. J. Muñoz-Batista, D. Motta Meira, G. Colón, A. Kubacka, M. Fernández-García, *Angew. Chem. Int. Ed.* **2018**, *130*, 1213–1217.

[37] B. Seemala, C. M. Cai, C. E. Wyman, P. Christopher, *ACS Catal.* **2017**, *7*, 4070–4082.

[38] G. Cha, P. Schmuki, M. Altomare, *Electrochim. Acta* **2017**, *258*, 302–310.

[39] K. Wasa, in *Handbook of Sputter Deposition Technology: Fundamentals and Applications for Functional Thin Films, Nano-Materials and MEMS: Second Edition*, Elsevier Inc., **2012**, pp. 41–75.

[40] Y. Koshtyal, D. Nazarov, I. Ezhov, I. Mitrofanov, A. Kim, A. Rymyantsev, O. Lyutakov, A. Popovich, M. Maximov, *Coating* **2019**, *9*, DOI 10.3390/coatings9050301.

[41] D. Tahir, S. Tougaard, *J. Phys. Condens. Matter* **2012**, *24*, DOI 10.1088/0953-8984/24/17/175002.

[42] L. Q. Wu, Y. C. Li, S. Q. Li, Z. Z. Li, G. D. Tang, W. H. Qi, L. C. Xue, X. S. Ge, L. L. Ding, *AIP Adv.* **2015**, *5*, DOI 10.1063/1.4931996.

[43] D. A. Cadenhead, N. J. Wagner, *J. Phys. Chem.* **1968**, *72*, 2775–2781.

[44] J. Sinfelt, J. Carter, D. Yates, *J. Catal.* **1972**, *24*, 283–296.

[45] S. H. Ahn, H. Y. Park, I. Choi, S. J. Yoo, S. J. Hwang, H. J. Kim, E. Cho, C. W. Yoon, H. Park, H. Son, J. M. Hernandez, S. W. Nam, T. H. Lim, S. K. Kim, J. H. Jang, *Int. J. Hydrogen Energy* **2013**, *38*, 13493–13501.

[46] W. Sheng, M. Myint, J. G. Chen, Y. Yan, *Energy Environ. Sci.* **2013**, *6*, 1509–1512.

[47] D. E. Eastman, *Phys. Rev. B* **1970**, *2*, 1–2.

[48] R. Ishii, K. Matsumura, A. Sakai, T. Sakata, *Appl. Surf. Sci.* **2001**, *169–170*, 658–661.

[49] I. Pašti, S. Mentus, *Mater. Chem. Phys.* **2009**, *116*, 94–101.

[50] Y. Shiraishi, H. Sakamoto, Y. Sugano, S. Ichikawa, T. Hirai, *ACS Nano* **2013**, *7*, 9287–9297.

[51] H. Yu, X. Huang, P. Wang, J. Yu, *J. Phys. Chem. C* **2016**, *120*, 3722–3730.

[52] M. Zhang, W. Zhong, Y. Xu, F. Xue, J. Fan, H. Yu, *J. Phys. Chem. Solids* **2021**, *149*, DOI 10.1016/j.jpcs.2020.109796.

[53] F. Du, H. Lu, S. Lu, J. Wang, Y. Xiao, W. Xue, S. Cao, *Int. J. Hydrogen Energy* **2018**, *43*, 3223–3234.

[54] Y. Xue, S. Min, J. Meng, X. Liu, Y. Lei, L. Tian, F. Wang, *Int. J. Hydrogen Energy* **2019**, *44*, 8133–8143.

[55] M. Rokhmat, E. Wibowo, Sutisna, Khairurrijal, M. Abdullah, *Procedia Eng.* **2017**, pp. 72–77.

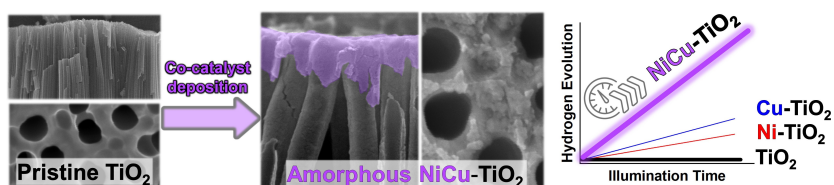[56] M. A. Bhosale, S. C. Karekar, B. M. Bhanage, *ChemistrySelect* **2016**, *1*, 6297–6307.

# RESEARCH ARTICLE

*M. Pinna, A. W. W. Wei, Dr. D. Spanu, Dr. J. Will, Dr. T. Yokosawa, Prof. Dr. E. Spiecker, Prof. Dr. S. Recchia, Prof. Dr. P. Schmuki, Dr. M. Altomare\**

**Amorphous NiCu Thin Films Sputtered on TiO₂ Nanotube Arrays: A Noble-Metal Free Photocatalyst for Hydrogen Evolution**

**A photocatalyst** consisting of an amorphous NiCu thin film sputtered on anodic TiO$_2$ nanotubes is studied for photocatalytic hydrogen evolution. A performance improvement of 4.6 and 3 times compared to photocatalysts modified with pure Ni or pure Cu films is achieved due to synergistic effect of Ni and Cu in the bimetallic co-catalyst layer.